SEMARAK ILMU PUBLISHING

Journal of Advanced Research in Fluid Mechanics and Thermal Sciences

Journal homepage:
https://semarakilmu.com.my/journals/index.php/fluid_mechanics_thermal_sciences/index
ISSN: 2289-7879

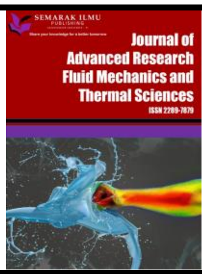

Analysis of Magneto Hydrodynamic Casson Nanofluid on an Inclined Porous Stretching Surface with Heat Source/Sink and Viscous Dissipation Effects: A Buongiorno Fluid Model Approach

Gobburu Sreedhar Sarma[1,*], Ganji Narender[1], Dontula Shankaraiah[1], Vishwaroju Ramakrishna[1], Gade Mallikarjun Reddy[1]

[1] Department of H&S (Mathematics), CVR College of Engineering, Hyderabad, India

ARTICLE INFO

Article history:
Received 29 June 2023
Received in revised form 30 August 2023
Accepted 13 September 2023
Available online 28 September 2023

Keywords:
Casson nanofluid; Magneto Hydrodynamic; Buongiorno fluid model; stretching surface

ABSTRACT

This study aims to investigate the characteristics of a magneto hydrodynamic Casson nanofluid flowing over a nonlinear inclined porous stretching surface when subjected to heat source/sink effects and viscous dissipation using a Buongiorno fluid model. Through the use of similarity transformations, nonlinear ODEs are derived from the governing nonlinear coupled PDEs and then solved using bvp4c solver in Mat lab. The outcomes of different physical parameters are shown graphically and tabulated to illustrate the changes in the velocity, temperature and concentration profiles. Additionally, numerical results for the Nusselt and Sherwood numbers are provided in tabular form. The correctness and validity of this study's findings are confirmed by a comparison to those found in the published literature. A higher rate of viscous dissipation and heat generation or absorption is associated with a lower heat transfer coefficient and a higher mass transfer coefficient, as shown by this investigation. This information could have implications for design and optimizing systems involving casson nanofluids and porous media, such as heat transfer systems, energy-efficient processes and catalytic reactions.

1. Introduction

Nanofluids are a relatively new type of fluid that consist of nanoparticles floating in a base fluid. Nanofluids have been discovered to improve the heat transfer coefficient between the heat transfer medium and the heat transfer surface, in contrast to conventional heat transfer fluids like water, ethylene glycol, and motor oil, which have poor thermal conductivity. On the other hand, experiments have demonstrated that nanofluids possess appreciably higher thermal conductivity than the base fluids. Choi and Eastman [1] pioneered the notion of "nanofluid." They noticed that adding nanoparticles to the base fluid increased its thermal conductivity substantially. This finding has led to extensive research on the use of nanofluids in various engineering applications. The

* *Corresponding author.*
E-mail address: sarma.sreedhar@gmail.com

https://doi.org/10.37934/arfmts.109.2.151167

nanoparticles commonly used include Al_2O_3, SiC, AlN, Cu, TiO and graphite, all of which exhibit strong thermal conductivity when compared to normal base fluids.

Buongiorno [2] has proposed a comprehensive mathematical model to study the thermal properties of nanofluids. Brownian motion and thermophoresis are identified as the two key processes for particle transfer in nanofluids that contribute to the base fluid's improved thermal conductivity. Brownian motion allows nanoparticles that move randomly within the base fluid to collide. The transfer of heat resulting from such collisions can significantly improve the thermal conductivity of nanofluids. Bakar *et al.,* [3] have analysed the mixed convection nanofluid flow in a porous medium. Viscoelastic nanofluid flow with constant heat flux was studied by Mahat *et al.,* [4]. Various other researchers have explored the influence of different parameters on nanofluids [5-9].

The Casson fluid model is a well-known mathematical model that is often employed to characterize the behaviour of non-Newtonian fluids. These fluids exhibit yield stress and are particularly relevant in industries such as biomechanics and polymer manufacturing. Casson fluids are commonly found in various everyday substances such as honey, jelly, soup, and tomato sauce. Various studies have investigated different aspects of Casson fluid behaviour, such as Falodun *et al.,* [10], who examined magneto-hydrodynamic heat and mass transfer through a vertical plate, and Dash *et al.,* [11] conducted a study on the flow of Casson fluids through a pipe containing a homogeneous porous media. Reddy *et al.,* [12] explored Brownian and thermophoretic properties of Casson fluid applying the Buongiorno model, while Kamran *et al.,* [13] conducted a numerical analysis of MHD flow in Casson nanofluids under slip boundary conditions and Joule heating. In their research, Khalid *et al.,* [14] explored the characteristics of unsteady magneto hydrodynamic free convection of Casson fluid flowing through a vertical plate that oscillated. Bejawada *et al.,* [15] was examined the magneto hydrodynamic casson fluid flow on an inclined nonlinear stretching surface with chemical reaction. The study of casson fluid flow with different parameter were explored by other researchers [16-18].

Current research is primarily focused on the flow of fluids through a sheet that is being stretched Crane [19]. The flow of a boundary layer that occurs as a result of either linear or nonlinear stretching of a sheet is a significant engineering problem with several applications in industry. These processes include the fabrication of rubber sheets, the extrusion of polymer sheets, hot rolling, wire drawing, production of glass fiber, better petroleum resource recovery, and cooling of large plates in a bath.

The quality of the end product is greatly influenced by the heat transfer process in the stretching sheet problem, which requires both cooling and heating. Several studies have investigated the flow behaviour of different types of fluids over various types of stretching sheets. In their study, Ullah *et al.,* [20] analysed the natural convection flow of Casson fluid with magneto-hydrodynamics over a surface that stretches non-linearly. Meanwhile, Narender *et al.,* [21] investigated a Casson fluid model with a radially stretching surface at the stagnation point. The effects of MHD flow of a Jeffery fluid through a stretching sheet was studied by Benal *et al.,* [22]. Considering a time-dependent stretching and nonlinear surface, Mukhopadhyay *et al.,* [23] and Mukhopadhyay [24] examined the flow of Casson fluid. Das *et al.,* [25] were examined a magneto radiated couple stress fluid over an exponentially stretching sheet under the influence of Ohmic dissipation. Sarkar *et al.,* [26] evaluated the entropy analysis of Magneto-Sisko nanofluid flow over a stretching and slipping cylinder. Asogwa *et al.,* [27] conducted a study on rheology of electromagnet hydrodynamic tangent hyperbolic nanofluid over stretching riga surface with different effects. Heat and mass transfer of Williamson nanofluid over a stretching surface was explored by Srinivasulu and Goud [28]. Many researchers studied the MHD flow of nanofluids over a stretched surface [17,29-32].

There has been an increasing interest in the investigation of nanofluid flow over a non-linear or linear stretching sheet in recent years, particularly under different conditions, including the implications of chemical reactions and viscous dissipation. Narender *et al.,* [33] conducted a study on MHD casson fluids through a stretching surface under the influence of dissipation and chemical reaction. Similar effects have also been studied by other researchers in the area of nanofluid flow through a stretching surface [34-37]. Additionally, Kamran [38] analysed the impact of heat generation or absorption on conventional micro polar fluid flow through a stretching surface. Sharanayya and Biradar [39] were analysed the dissipative casson nanofluid flow past a stretching sheet with heat generation or absorption. Using finite element analysis, the effect of heat source on an unsteady magneto hydrodynamic flow of casson fluid through an oscillating plate was analysed by Goud *et al.,* [40]. Reddy *et al.,* [41] were examined the effect of heat source or sink on MHD fluid flow along a stretching cylinder.

Drawing from the literature discussed above, the primary goal of this investigation is to extend the work of Reddy *et al.,* [12] to examine the characteristics of the flow of a two-dimensional, incompressible Casson nanofluid over a porous stretching sheet inclined at a nonlinear angle. The analysis incorporates the effects of viscous dissipation and heat generation or absorption. By utilizing similarity transformations, the boundary layer equations were converted into nonlinear ODEs, which were then solved using a numerical algorithm in Matlab. The study explores how several dimensionless parameters affect the behaviour of the flow and the results are shown in the form of tables and graphs.

2. Mathematical Analysis

Consider the flow of an incompressible Casson nanofluid through a porous stretching surface in two dimensions. The surface is inclined at an angle α and is subject to both extending speed $u_w(x) = ax^m$ and free stream speed $u_\infty(x) = 0$. Transverse magnetic field B_0 is applied normal to the flow. The wall temperature T_w and nanoparticle fraction C_w are prescribed at the wall. Using the temperature T_f and the heat exchange factor h_f proportional to x^{-1}, the effects of thermal radiation are taken into account via convective heating. The temperature distribution T_∞ and mass transfer distribution C_∞ of the nanofluid are obtained as y tends to infinity, from Figure 1.

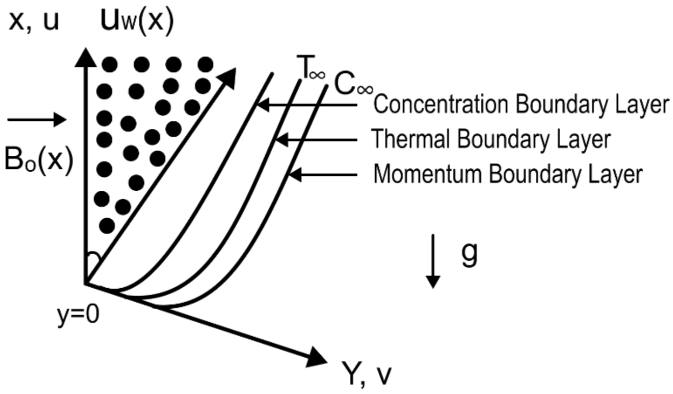

Fig. 1. Physical Model

The behaviour of a Casson fluid in isotropic motion can be described by the constitutive equation:

$$\tau_{ij} = \begin{cases} 2\left(\mu_B + \dfrac{P_y}{\sqrt{2\pi}}\right)e_{ij}, & \pi > \pi_c \\ 2\left(\mu_B + \dfrac{P_y}{\sqrt{2\pi_c}}\right)e_{ij}, & \pi < \pi_c \end{cases} \tag{1}$$

From Eq. (1), $\pi = e_{ij}e_{ij}$ where e_{ij} denotes (*i*, *j*) th component of the deformation rate. This indicates that π is a representation of a deformation rate component multiplied by itself. According to the non-Newtonian paradigm, π_c denotes a critical value of this product.

The paper examines the Buongiorno model and its application to the Casson fluids, which is a type of non-Newtonian fluid used to describe substances like jelly, honey, fruit juices, soup and blood. Casson fluids are characterized by a yield stress, infinite viscosity at low shear rates, and near-zero viscosity at extremely high shear rates, as well as by their shear-thinning characteristics.

The equations describing the flow are as follows [12]:

$$\frac{\partial \bar{u}}{\partial x} + \frac{\partial \bar{v}}{\partial y} = 0 \tag{2}$$

$$\bar{u}\frac{\partial \bar{u}}{\partial x} + \bar{v}\frac{\partial \bar{u}}{\partial y} = \nu\left(1+\frac{1}{\beta}\right)\frac{\partial^2 \bar{u}}{\partial y^2} + g\left[\beta_T(\bar{T}-T_\infty)+\beta_C(\bar{C}-C_\infty)\right]\cos\alpha - \frac{\sigma B_0^{\,2}(x)}{\rho}\bar{u} - \frac{\nu}{K}\bar{u} \tag{3}$$

$$\begin{aligned} \bar{u}\frac{\partial \bar{T}}{\partial x} + \bar{v}\frac{\partial \bar{T}}{\partial y} &= \frac{\kappa}{\rho C_p}\frac{\partial^2 \bar{T}}{\partial y^2} - \frac{1}{(\rho c)_f}\frac{\partial q_r}{\partial y} + \tau\left[D_B\frac{\partial \bar{C}}{\partial y}\frac{\partial \bar{T}}{\partial y} + \frac{D_T}{T_\infty}\left(\frac{\partial \bar{T}}{\partial y}\right)^2\right] \\ &\quad + \frac{\mu}{\rho C_p}\left(1+\frac{1}{\beta}\right)\left(\frac{\partial \bar{u}}{\partial y}\right)^2 - \frac{Q_0}{\rho C_p}(\bar{T}-T_\infty) \end{aligned} \tag{4}$$

$$\bar{u}\frac{\partial \bar{C}}{\partial x} + \bar{v}\frac{\partial \bar{C}}{\partial y} = D_B\frac{\partial^2 \bar{C}}{\partial y^2} + \frac{D_T}{T_\infty}\frac{\partial^2 \bar{T}}{\partial y^2} - K_r(\bar{C}-C_\infty) \tag{5}$$

The B.Cs are defined as:

$$\begin{aligned} &\bar{u} = u_w(x) = ax^m;\ \bar{v} = 0;\ -k\frac{\partial \bar{T}}{\partial y} = h_f\left[T_f - \bar{T}\right];\ \bar{C} = C_w \quad \text{at } y = 0 \\ &\bar{u} \to u_\infty(x) = 0;\ \bar{v} \to 0;\ \bar{T} \to T_\infty;\ \bar{C} \to C_\infty \quad \text{as} \quad y \to \infty \end{aligned} \tag{6}$$

The formula for calculating the Roseland flux is:

$$q_r = -\frac{4\sigma^*}{3k^*}\frac{\partial T^4}{\partial y} \tag{7}$$

Using the Taylor series of $\bar{T}^4$ around the free stream T_∞ by ignoring the higher order terms and the local temperature $\bar{T}$ and the free stream have very little variation in temperature.

$$\bar{T}^4 \cong 4T_\infty{}^3\bar{T} - 3T_\infty{}^4 \tag{8}$$

Eq. (7) and Eq. (8) can be used to simplify Eq. (4) to:

$$\bar{u}\frac{\partial \bar{T}}{\partial x} + \bar{v}\frac{\partial \bar{T}}{\partial y} = \left[\alpha + \frac{16\sigma^* T_\infty{}^3}{3k^*(\rho c)_f}\right]\frac{\partial^2 \bar{T}}{\partial y^2} + \tau\left[D_B\frac{\partial \bar{C}}{\partial y}\frac{\partial \bar{T}}{\partial y} + \frac{D_T}{T_\infty}\left(\frac{\partial \bar{T}}{\partial y}\right)^2\right]$$
$$+\frac{\mu}{\rho C_p}\left(1+\frac{1}{\beta}\right)\left(\frac{\partial \bar{u}}{\partial y}\right)^2 - \frac{Q_0}{\rho C_p}(\bar{T} - T_\infty) \tag{9}$$

$\tau = \frac{(\rho c)_p}{(\rho c)_f}$ represents the relationship among the nanoparticle' heat capacity and the heat capacity of liquid.

Using the below similarity transformations as:

$$\psi = \sqrt{\frac{2\upsilon a x^{m+1}}{m+1}};\quad \theta(\eta) = \frac{\bar{T} - T_\infty}{T_w - T_\infty};\quad \phi(\eta) = \frac{\bar{C} - C_\infty}{C_w - C_\infty};\ \eta = y\sqrt{\frac{(m+1)a x^{m-1}}{2\upsilon}} \tag{10}$$

where $\psi(x, y)$ stream function satisfying

$$\bar{u} = \frac{\partial \psi}{\partial y},\qquad \bar{v} = -\frac{\partial \psi}{\partial x} \tag{11}$$

Eq. (2) is satisfied by using Eq. (10) and Eq. (11) and Eq. (3), Eq. (5) and Eq. (9) are translated into the subsequent ODEs:

$$\left(1+\frac{1}{\beta}\right)\frac{d^3 f}{d\eta^3} + f(\eta)\frac{d^2 f}{d\eta^2} - \frac{2m}{m+1}\left(\frac{df}{d\eta}\right)^2 + \frac{2}{m+1}\left(\lambda\theta(\eta) + \delta\phi(\eta)\right)\cos\alpha - \frac{2}{m+1}\left(M + \frac{1}{K}\right)\frac{df}{d\eta} = 0 \tag{12}$$

$$\frac{1}{\Pr}\left(1+\frac{4}{3}R\right)\frac{d^2\theta}{d\eta^2} + f(\eta)\frac{d\theta}{d\eta} + Nb\frac{d\theta}{d\eta}\frac{d\phi}{d\eta} + Nt\left(\frac{d\theta}{d\eta}\right)^2 + \left(1+\frac{1}{\beta}\right)Ec\left(\frac{d^2 f}{d\eta^2}\right)^2 + Q\theta(\eta) = 0 \tag{13}$$

$$\frac{d^2\phi}{d\eta^2}+Le\,f(\eta)\ \frac{d\phi}{d\eta}+\left(\frac{Nt}{Nb}\right)\ \frac{d^2\theta}{d\eta^2}-Kr\ Le\ \phi(\eta)=0 \tag{14}$$

The associated B.Cs are changed as:

$$\begin{aligned}&f(\eta)=0;\ \frac{df}{d\eta}=1;\ \frac{d\theta}{d\eta}=-Bi(1-\theta(0));\ \phi(\eta)=1\quad \text{at}\quad \eta=0\\&\frac{df}{d\eta}\to 0;\ \theta(\eta)\to 0;\ \phi(\eta)\to 0\qquad \text{as}\quad \eta\to\infty\end{aligned} \tag{15}$$

The following are the important parameters:

$$P_r=\frac{\nu}{\alpha},\ Le=\frac{\nu}{D_B},Nb=\frac{(\rho c)_p D_B(C_w-C_\infty)}{(\rho c)_f\,\nu},Nt=\frac{(\rho c)_p D_T(T_w-T_\infty)}{(\rho c)_f\,\nu T_\infty}$$

$$M=\frac{\sigma B_0{}^2(x)x}{\rho u_w},Ec=\frac{u^2}{C_p(T_f-T_\infty)},\lambda=\frac{Gr}{\mathrm{Re}_x{}^2},\delta=\frac{Gc}{\mathrm{Re}_x{}^2},K=\frac{K_1u_w}{\nu x}$$

$$R=\frac{4\sigma^* T_\infty{}^3}{k^*K},Gr=\frac{g\beta_T(T_w-T_\infty)x^3}{\nu^2},Gc=\frac{g\beta_C(C_w-C_\infty)x^3}{\nu^2},Kr=\frac{2xK_r}{(m+1)u_w},$$

$$Q=\frac{Q_0}{\rho C_p},\mathrm{Re}_x=\frac{u_w x}{\nu},Bi=\frac{\eta}{k\sqrt{\mathrm{Re}_x}}$$

In this paper, the parameters of the skin friction coefficient, Nusselt number and Sherwood number are investigated.

$$C_f=\frac{\tau_w}{u_w{}^2\rho f},Nur=\frac{xq_w}{k(T_w-T_\infty)},Shr=\frac{xq_m}{D_B(C_w-C_\infty)}$$

$$\text{where}\ \ q_w=-\left[k+\frac{4\sigma^* T_\infty{}^3}{3k^*}\right]\frac{\partial T}{\partial y},q_m=-D_B\frac{\partial C}{\partial y},\tau_w=\mu\left(1+\frac{1}{\beta}\right)\frac{\partial u}{\partial y}\ \text{at}\ y=0$$

Nusselt number is denoted by $-\theta'(0)$, Sherwood number by $-\phi'(0)$ and the skin friction denoted by $C_f=\left(1+\dfrac{1}{\beta}\right)f''(0)$ and they are defined as follows:

$$-\theta'(0)=\frac{Nur}{\left(1+\frac{4}{3}R\right)\sqrt{\left(\frac{m+1}{2}\right)\mathrm{Re}_x}};\ \ -\phi'(0)=\frac{Shr}{\sqrt{\left(\frac{m+1}{2}\right)\mathrm{Re}_x}};\ C_f=C_f\sqrt{\left(\frac{m+1}{2}\right)\mathrm{Re}_x}$$

3. Solution of the Problem

Numerical solutions for the ODEs Eq. (12) to Eq. (14) subject to the BCs Eq. (15) are solved by using the bvp4c solver in MATLAB. The three-stage Lobatto IIIa formula is implemented by the solver, a finite difference algorithm with fourth order precision. It employs a collocation approach to approximate the solution. Collocation involves discretizing the domain into a set of collocation points and then satisfying the ODEs at these points. In order to implement the solver, the coupled ODEs Eq. (12) to Eq. (14) are converted into system of first order ODEs as follows.

Let

$$
\begin{aligned}
& f = y_1, \frac{df}{d\eta} = y_2, \frac{d^2 f}{d\eta^2} = y_3, \theta = y_4, \frac{d\theta}{d\eta} = y_5, \phi = y_6, \frac{d\phi}{d\eta} = y_7 \\
& y_1' = y_2, \\
& y_2' = h_3, \\
& y_3' = \frac{\beta}{1+\beta}\left[-y_1 y_3 + \left(\frac{2m}{m+1}\right) y_2^{\,2} - \left(\frac{2}{m+1}(\lambda y_4 + \delta y_6)\right)\cos\alpha \right) + \frac{2}{m+1}\left(M + \frac{1}{K}\right) y_2 \right], \\
& y_4' = y_5, \\
& y_5' = \frac{3\Pr}{3+4R}\left[-y_1 y_5 - Nb y_5 y_7 - Nt y_5^{\,2} - \left(1 + \frac{1}{\beta}\right) Ec y_3^{\,2} - Q y_4 \right], \\
& y_6' = y_7, \\
& y_7' = -Le y_1 y_7 - \left(\frac{Nt}{Nb}\right) y_5' + Kr\ Le y_6
\end{aligned} \tag{16}
$$

the corresponding boundary conditions are.

$$
\begin{aligned}
& y_1(0) = 0,\ y_2(0) = 1,\ y_5(0) = -Bi(1 - y_4(0)),\ y_6(0) = 0, \quad \eta = 0 \\
& y_2(\eta) \to 0,\ y_4(\eta) \to 0,\ y_6(\eta) \to 0 \quad \text{as } \eta \to \infty
\end{aligned}
$$

To ensure the accuracy and credibility of the solutions, they are compared with previously published results as a benchmark. To analyse the findings, dimensionless parameters are displayed on profiles of velocity, temperature, and concentration. Nur and Shr are calculated for various non dimensional parameters which are given in a tabular format.

4. Outcomes and Interpretation

This study presents graphical and tabulated forms of numerical results for a number of physical parameters, including Magnetic number M, thermal buoyancy parameter λ, solutal buoyancy parameter δ, inclination angle α, Permeability parameter K, Radiation parameter R, Prandtl number $\Pr$, Casson parameter β, Eckert number Ec, Chemical reaction parameter Kr, Brownian motion Nb, Thermophoresis parameter Nt, Heat generation or absorption parameter Q, Lewis number Le, and Biot number Bi. The values of Nur and Shr are compared with the outcomes from a prior study Reddy *et al.,* [12] to ensure that the numerical algorithm used in this study is valid. The comparison reveals good agreement between the outcomes produced by the current algorithm and those in Table 1. produced by Reddy *et al.,* [12]. A numerical examination of the impact of the Eckert number and the heat generation or absorption parameter on the local Nusselt and Sherwood numbers is also provided in Table 2. The findings indicate that when Eckert number and Heat source/sink parameter grow, Nusselt number decreases while Sherwood number increases.

Table 1
Comparison of the present results with Reddy *et al.,* [12] on Reduced Nusselt number Nur and Reduced Sherwood number Shr when Ec = 0, Q = 0

m	M	β	$\Pr$	R	Nb	Kr	α	Bi	Nur		Shr	
									Reddy *et al.,* [12]	Present Outcome	Reddy *et al.,* [12]	Present Outcome
1	0.5	0.5	0.71	1	0.1	0.5	π/4	0.1	0.072799	0.0726955	2.1317242	2.1316321
2									0.073107	0.0730052	2.1440112	2.1440114
3									0.073466	0.0734110	2.1576123	2.1576233
4									0.073892	0.0737591	2.1728725	2.1727651
1	1	0.5	0.71	1	0.1	0.5	π/4	0.1	0.074017	0.0739121	2.174142	2.1741222
	2								0.074168	0.0749002	2.175710	2.1749211
	3								0.074254	0.0741922	2.176629	2.1765822
	4								0.074311	0.0742911	2.177230	2.1771121
1	0.5	0.5	0.71	1	0.1	0.5	π/4	0.1	0.072833	0.0728331	2.133445	2.1334512
		1							0.073013	0.0730133	2.140694	2.1406942
		1.5							0.073314	0.0733142	2.152397	2.1523972
		2							0.073928	0.0739280	2.174682	2.1746829
1	0.5	0.5	6	1	0.1	0.5	π/4	0.1	0.089083	0.0882321	2.153118	2.1529541
			7						0.089796	0.0890212	2.153932	2.1538711
			8						0.090348	0.0899121	2.154921	2.1540021
			9						0.090789	0.0907890	2.156133	2.1551215
1	0.5	0.5	7	1	0.1	0.5	π/4	0.1	0.083620	0.0835912	2.154921	2.1548922
				2					0.085402	0.0854001	2.158643	2.1586004
				3					0.087457	0.0874123	2.161399	2.1612981
				4					0.089796	0.0897002	2.163519	2.1635194
1	0.5	0.5	7	1	0.1	0.5	π/4	0.1	0.081929	0.0819281	2.154921	2.1549112
					0.2				0.085064	0.0850635	2.171138	2.1711290
					0.3				0.087661	0.0876600	2.177223	2.1772119
					0.4				0.089796	0.0897961	2.180837	2.1808291
1	0.5	0.5	7	1	0.1	0.5	π/4	0.1	0.089434	0.088921	2.154921	2.1539321
						1			0.089517	0.089002	2.678377	2.6772321
						1.5			0.089630	0.088914	3.115223	3.1152230
						2			0.089796	0.089003	3.497552	3.4975422
1	0.5	0.5	7	1	0.1	0.5	π/6	0.1	0.089515	0.089500	2.137252	2.1371331
							π/4		0.089718	0.089720	2.149859	2.1498590
							π/3		0.089796	0.089735	2.154921	2.1548221
							π/2		0.089853	0.089921	2.158746	2.1584670
1	0.5	0.5	7	1	0.1	0.5	π/4	0.1	0.089796	0.088921	2.114918	2.1148541
								0.2	0.162697	0.161921	2.125481	2.1253914
								0.3	0.222809	0.222901	2.138521	2.1384899
								0.4	0.273073	0.272990	2.154921	2.1549007

Table 2
Outcomes of Nur and Shr for varied values of Ec and Q

Ec	Q	Nur	Shr
0.1		0.0612107	2.2335
0.2		0.0510758	2.25797
0.3		0.0415928	2.28079
0.4		0.0326763	2.30217
	-0.1	0.0685859	2.22119
	0	0.06541	2.22657
	0.1	0.0612107	2.2335
	0.2	0.0553904	2.2429

Effects of Magnetic Number M and Permeable Parameter K are shown in Figure 2. The findings show that a decrease in velocity profiles is brought on by an increase in magnetic number. This is because the fluid flow has been impeded by the introduction of a transverse magnetic field. A higher value for the Permeable parameter enhances the velocity profiles by enlarging the holes and allowing more room for fluid particles to move freely. Permeability describes how fluid particles move across different regions of the boundary layer.

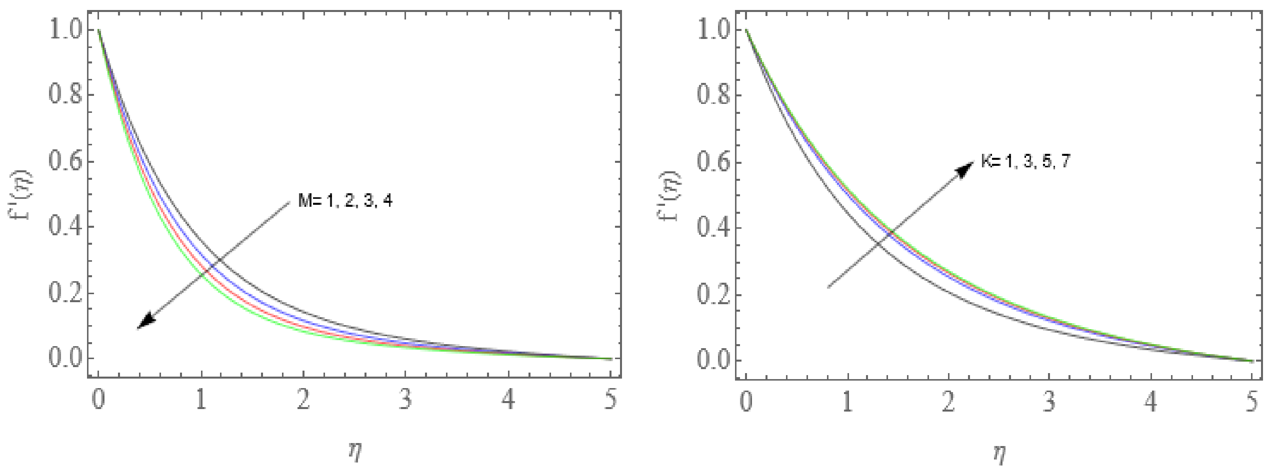

Fig. 2. Impact of M and K on Velocity Profile f'

The implications of the Casson parameter β and power index parameter m on the velocity profiles is illustrated in Figure 3. The higher values of β correspond to an increase in fluid velocity, which results in a drop in the yield stress and a reduction in the thickness of the momentum boundary layer. As a result, the velocity profiles get flatter as the Casson parameter increases. Increases in m cause the velocity profiles ascend due to stronger shear thinning behaviour of the fluid. Viscosity decreases as the shear rate increases which results the increase in fluid velocity.

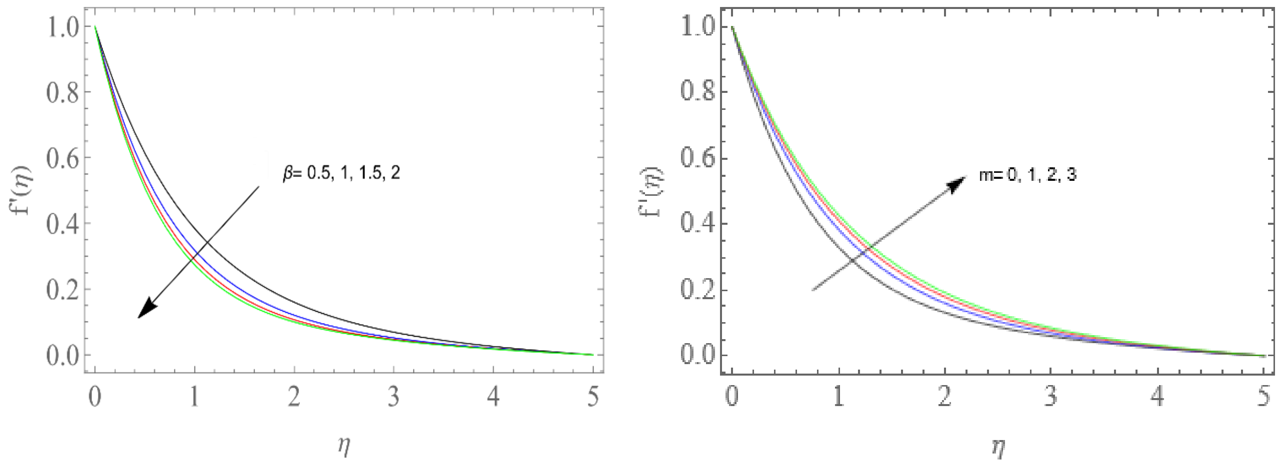

Fig. 3. Effect of β and m on Velocity Profile f'

Figure 4 illustrates how solutal buoyancy δ and thermal buoyancy λ affect fluid movement. The findings indicate that a higher value of these parameters results in a stronger buoyancy force, which reduces fluid viscosity and accelerates fluid movement, leading to enhanced velocity profiles. Meanwhile, the impact of the inclination factor α can be observed from Figure 5. Due to the existence of a magnetic field that hinders fluid flow, the velocity profiles drop as the inclination factor rises. Additionally, the velocity profile experiences a greater decline when the value of $\alpha = \dfrac{\pi}{2}$.

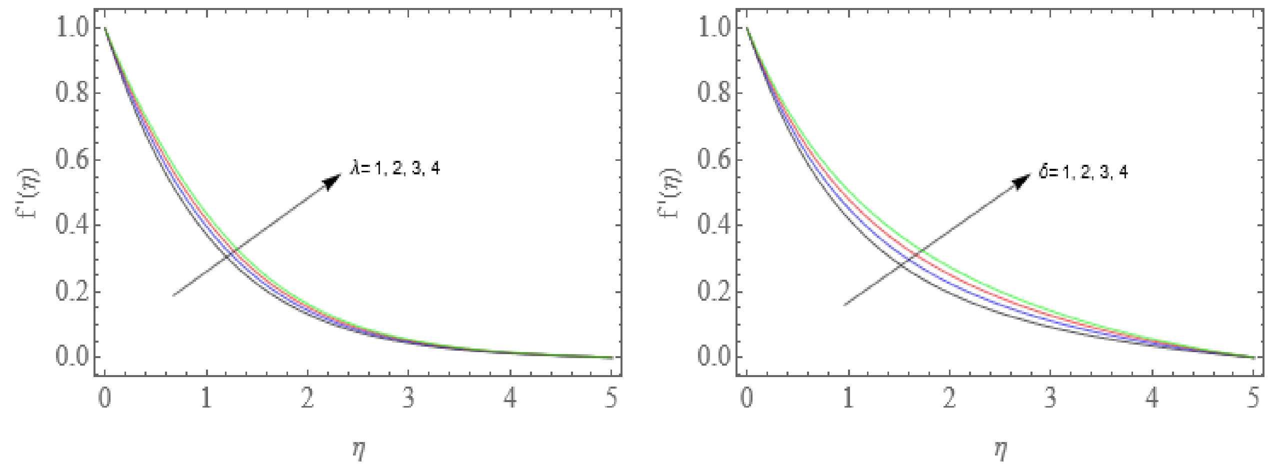

Fig. 4. Impact of λ and δ on Velocity Profile f'

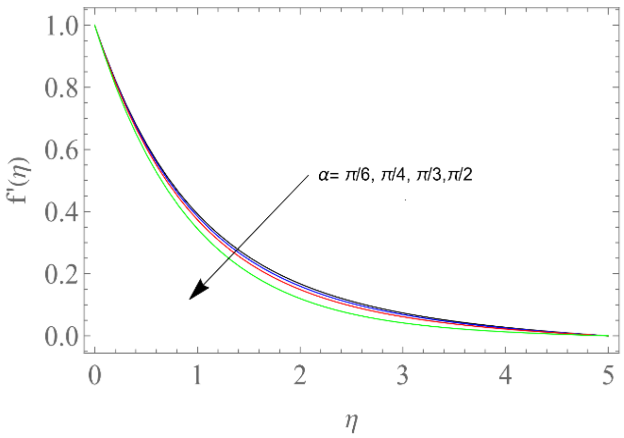

Fig. 5. Impact of α on Velocity Profile f'

In Figure 6, we see the impact of changing both the radiation parameter R and the Prandtl number Pr .When R is increased, the profiles of temperature drop close to the boundary and rise at the distant distance. This is because an increase in the Radiation parameter causes the fluid's temperature to rise and in turn, causes the boundary layer to thicken. The thermal diffusivity to momentum diffusivity ratio is quantified by the Prandtl number. The temperature profile first rises close to the boundary as the Prandtl number rises, then falls away from the boundary.

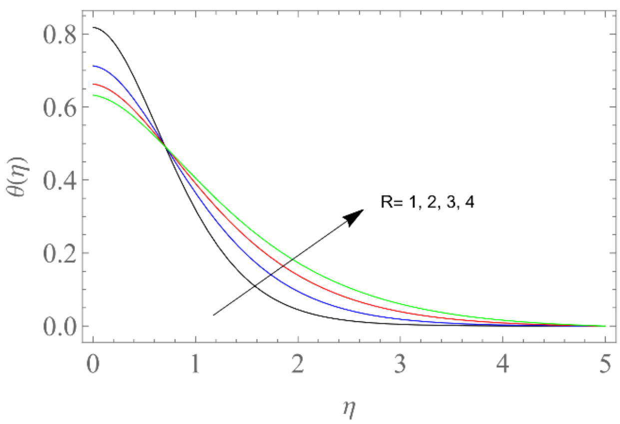

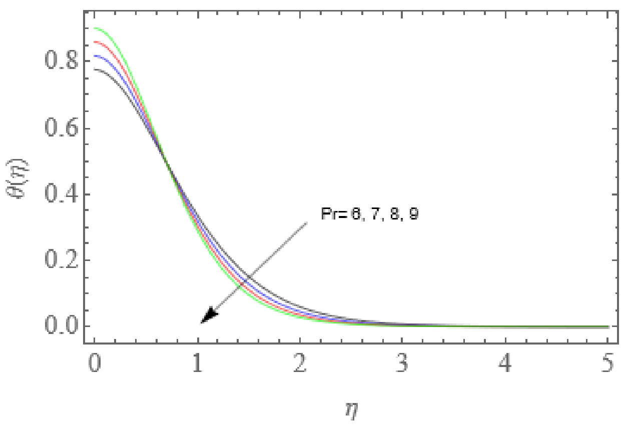

Fig. 6. Effect of R and Pr on Temperature Profile θ

Figure 7 demonstrates the outcomes of Nb and Nt. Due to the enhancement in the kinetic energy and movement of the nanoparticles, the temperature climbs, and the thickness of the thermal boundary layer grows as the Brownian motion parameter Nb increases. The temperature profile also increases as the Thermophoresis parameter increases because heated particles move away from higher temperatures to lower temperatures, leading to an overall temperature increase in the fluid.

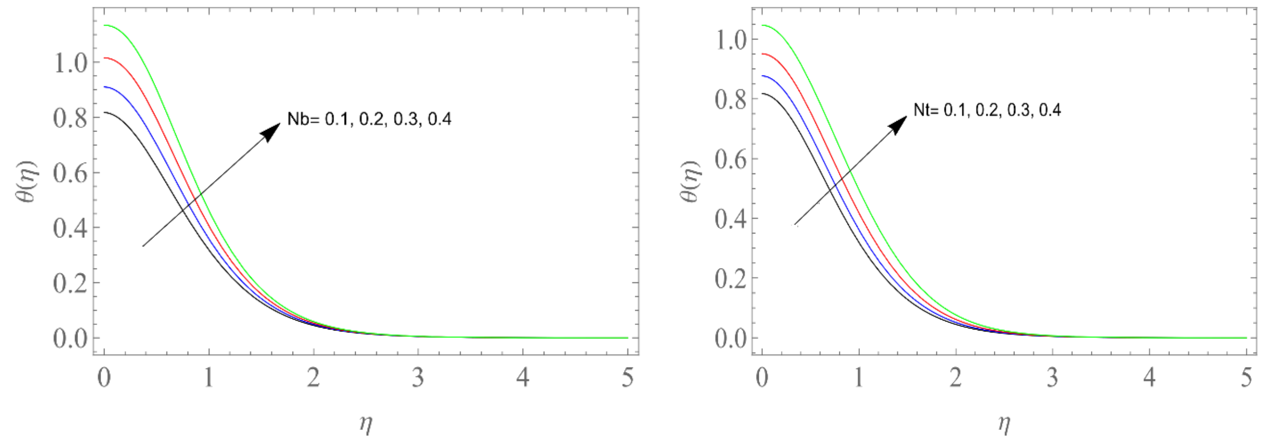

Fig. 7. Impact of Nb and Nt on Temperature Profile θ

The impacts of the heat generation or absorption parameter Q and the Eckert number Ec are described in Figure 8. More energy may be stored in a fluid region with a higher value of viscous dissipation. This viscous dissipation leads to the generation of heat due to fractional heating, resulting in elevated temperature profiles. More heat is produced with an increase in Q ($Q > 0$), which raises the temperature and thickens the thermal boundary layer. However, as Q degenerates ($Q < 0$), the heat absorbed causes a decrease in temperature and a thickening of the thermal boundary layer.

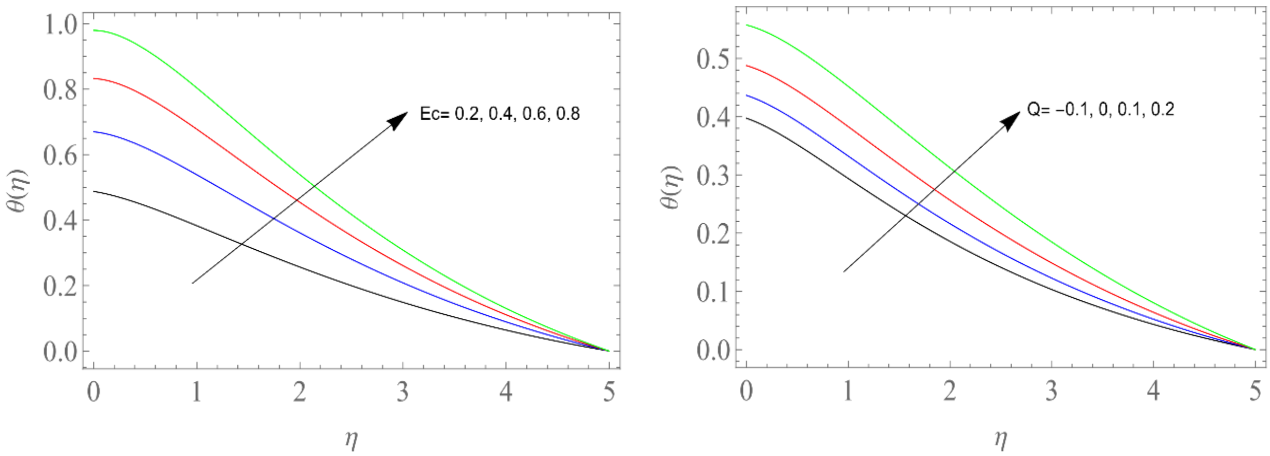

Fig. 8. Effect of Ec and Q on Temperature Profile θ

The findings of the Biot number Bi and inclination factor α are shown in Figure 9. The Biot number is a measure of how much thermal resistance there is for convection at a body's surface compared to thermal resistance for conduction within the body. The temperature profile rises as a consequence of increased sheet convective heating, as seen in the figure, which is caused by rising Biot number. Like this, raising the inclination factor also causes the temperature profile to rise.

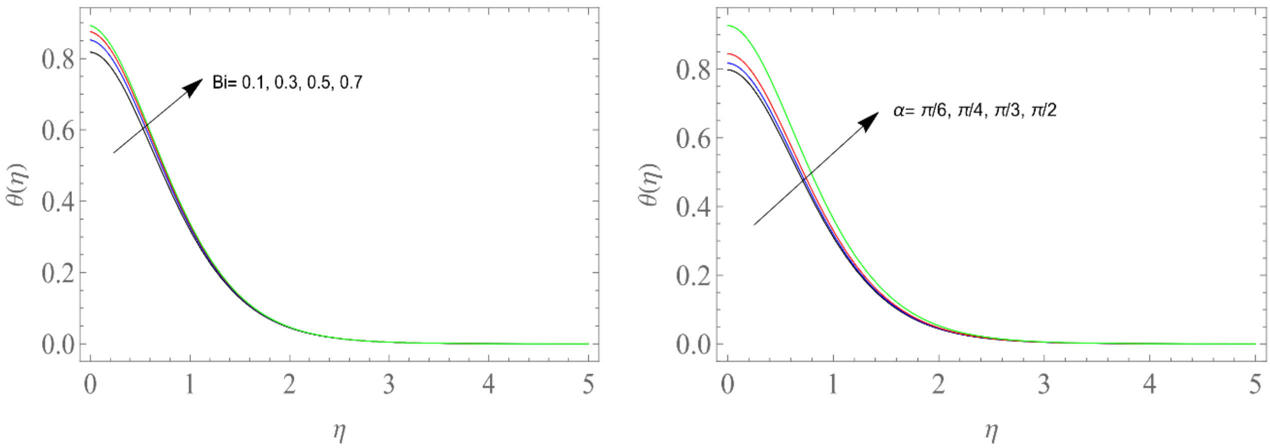

Fig. 9. Impact of Bi and α on Temperature Profile θ

The outcomes of Nb and Nt are shown in Figure 10. The fluid concentration and boundary layer thickness both drop when the Brownian motion parameter is increased. Increases in the Thermophoresis parameter cause the fluid concentration to fall close to the boundary but rise further away from it, increasing the thickness of the boundary layer.

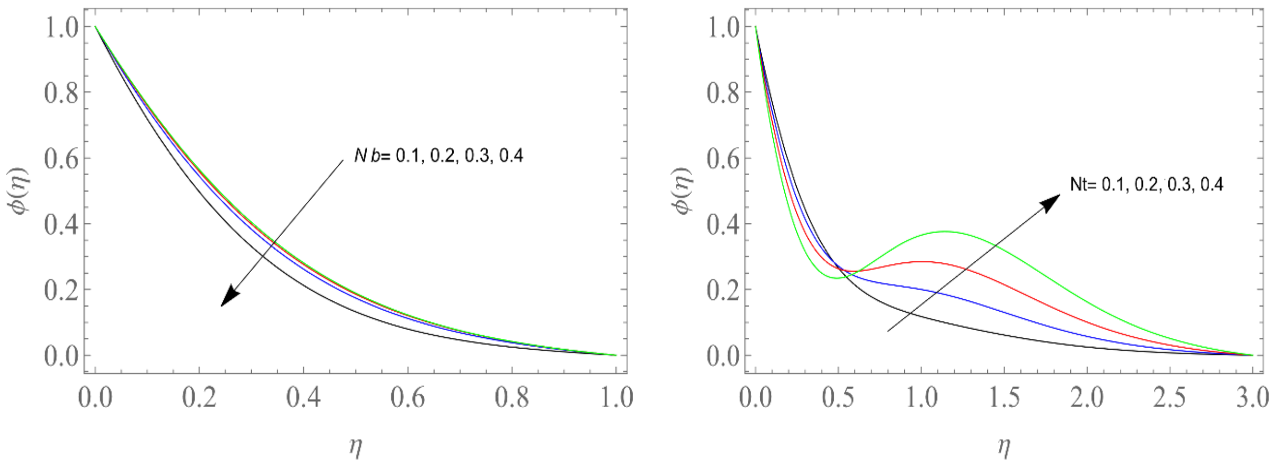

Fig. 10. Impact of Nb and Nt on Concentration Profile ϕ

Figure 11 depicts the influence of the Kr and Le. The concentration profile is shown to be negatively impacted by an increase in the chemical reaction parameter. It is also shown that the Lewis number, a dimensionless quantity that establishes the ratio of species to thermal diffusion rates, has an effect. When the Lewis number increases, it indicates that the rate of thermal diffusion is higher compared to species diffusion in a fluid mixture. This means that heat is transported more rapidly than the species, resulting in a steeper temperature gradient in comparison to the concentration gradient. Therefore, the concentration boundary layer becomes thinner. The effect of Ec on Nusselt number and Sherwood number is depicted in Figure 12. It observed that, as Eckert number increases, Nusselt number decreases and Sherwood number increases. From Figure 13, it is seen that, for increasing values of heat source or sink parameter Q, Nusselt number decreases whereas Sherwood number increases.

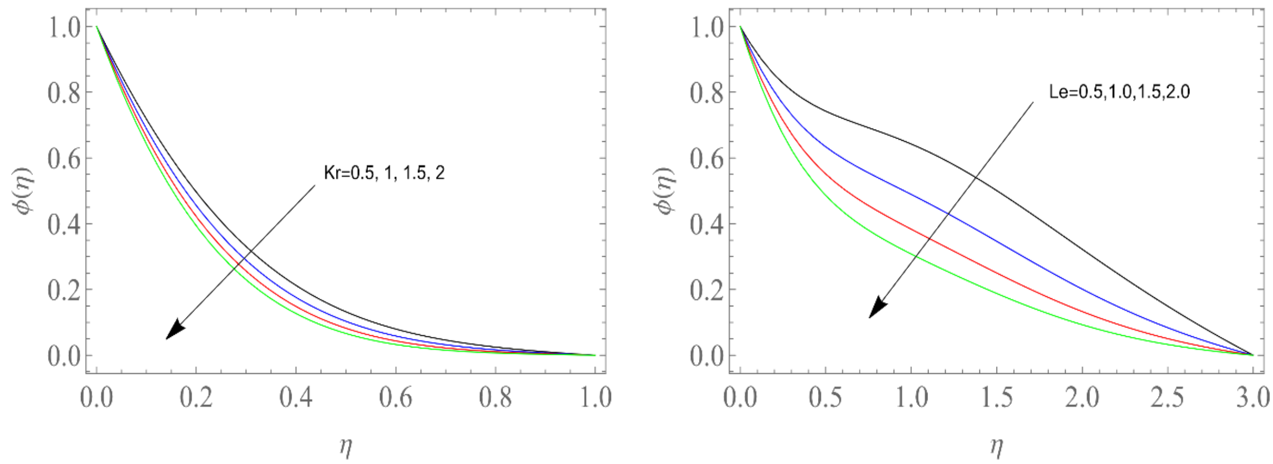

Fig. 11. Effect of Kr and Le on Concentration Profile ϕ

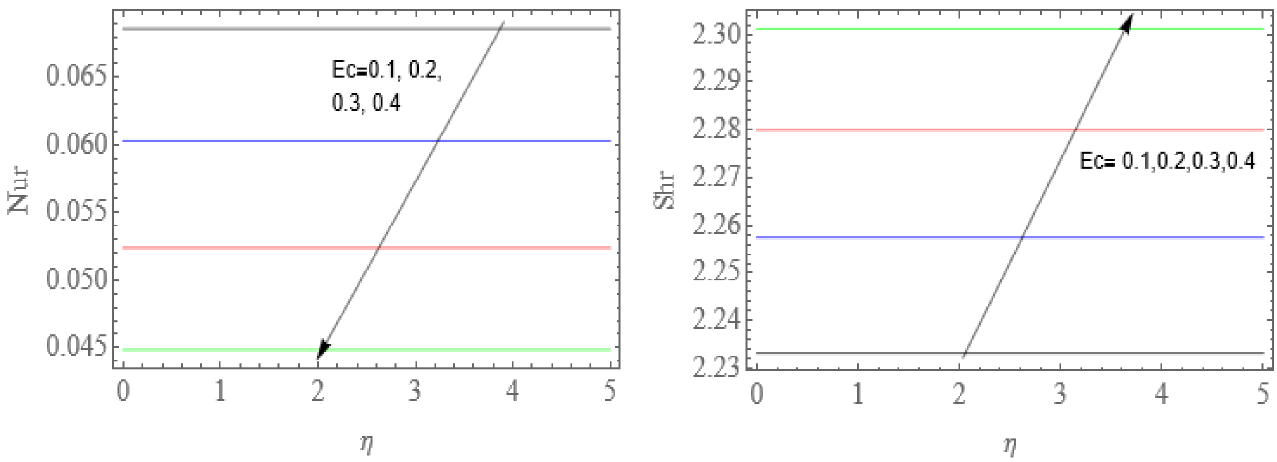

Fig. 12. Effect of Ec on Nur and Shr

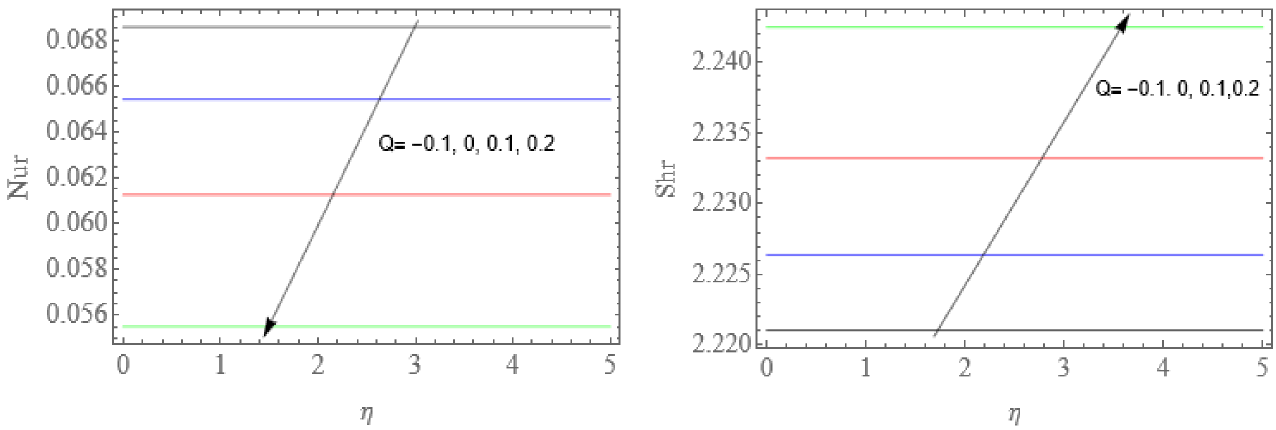

Fig. 13. Effect of Q Nur and Shr

5. Conclusions

After considering all the arguments and results, we have compiled our findings in the following summary:

i. As the fluid's thermal conductivity increases with increasing dissipation, a rise in the Eckert number Ec leads to a higher temperature profile.

ii. A positive value for the heat source/sink parameter Q means that more heat is produced in the system, leading to a higher temperature and a thicker thermal boundary layer. If Q is negative, the system absorbs heat, causing the temperature and the thickness of the thermal boundary layer to drop.
iii. As the Radiation parameter R rises, so does the temperature profile.
iv. As Brownian motion increases, the thermal boundary layer thickens, and the concentration boundary layer thins.
v. When the Thermophoresis parameter Nt is raised, a rise also occurs in the concentration and temperature profiles.
vi. The velocity profiles get flatter when inclination angle α is increased.
vii. Raising the Casson parameter in a Casson fluid results in a decrease in fluid velocity.

The results obtained in this study will be used to analyse the heat and mass transport features in many non-Newtonian nano fluid flow industrial applications. This work can be extended in future with some other geometries and physical conditions.

Acknowledgement
We are grateful that the reviewer's spent the time and proceeded to read the article. We really appreciate your insightful comments and recommendations, which helped us improve the content of the article. This research was not funded by any grant.

References
[1] Choi, S. US, and Jeffrey A. Eastman. *Enhancing thermal conductivity of fluids with nanoparticles*. No. ANL/MSD/CP-84938; CONF-951135-29. Argonne National Lab.(ANL), Argonne, IL (United States), 1995.
[2] Buongiorno, Jacopo. "Convective transport in nanofluids." *ASME Journal of Heat and Mass Transfer* 128, no. 3 (2006): 240-250. https://doi.org/10.1115/1.2150834
[3] Bakar, Shahirah Abu, Norihan Md Arifin, and Ioan Pop. "Stability Analysis on Mixed Convection Nanofluid Flow in a Permeable Porous Medium with Radiation and Internal Heat Generation." *Journal of Advanced Research in Micro and Nano Engineering* 13, no. 1 (2023): 1-17. https://doi.org/10.37934/armne.13.1.117
[4] Mahat, Rahimah, Muhammad Saqib, Imran Ulah, Sharidan Shafie, and Sharena Mohamad Isa. "MHD Mixed Convection of Viscoelastic Nanofluid Flow due to Constant Heat Flux." *Journal of Advanced Research in Numerical Heat Transfer* 9, no. 1 (2022): 19-25.
[5] Nandi, Susmay, Manik Das, and Bidyasagar Kumbhakar. "Entropy Generation in Magneto-Casson Nanofluid Flow Along an Inclined Stretching Sheet Under Porous Medium with Activation Energy and Variable Heat Source/Sink." *Journal of Nanofluids* 11, no. 1 (2022): 17-30. https://doi.org/10.1166/jon.2022.1823
[6] Sarkar, S., R. N. Jana, and S. Das. "Activation energy impact on radiated magneto-Sisko nanofluid flow over a stretching and slipping cylinder: entropy analysis." *Multidiscipline Modeling in Materials and Structures* 16, no. 5 (2020): 1085-1115. https://doi.org/10.1108/MMMS-09-2019-0165
[7] Shankar Goud, Bejawada, Yanala Dharmendar Reddy, and Satyaranjan Mishra. "Joule heating and thermal radiation impact on MHD boundary layer Nanofluid flow along an exponentially stretching surface with thermal stratified medium." *Proceedings of the Institution of Mechanical Engineers, Part N: Journal of Nanomaterials, Nanoengineering and Nanosystems* (2022): 23977914221100961. https://doi.org/10.1177/23977914221100961
[8] Bejawada, Shankar Goud, and Mahantesh M. Nandeppanavar. "Effect of thermal radiation on magnetohydrodynamics heat transfer micropolar fluid flow over a vertical moving porous plate." *Experimental and Computational Multiphase Flow* 5, no. 2 (2023): 149-158. https://doi.org/10.1007/s42757-021-0131-5
[9] Bejawada, Shankar Goud, Yanala Dharmendar Reddy, Wasim Jamshed, Mohamed R. Eid, Rabia Safdar, Kottakkaran Sooppy Nisar, Siti Suzilliana Putri Mohamed Isa, Mohammad Mahtab Alam, and Shahanaz Parvin. "2D mixed convection non-Darcy model with radiation effect in a nanofluid over an inclined wavy surface." *Alexandria Engineering Journal* 61, no. 12 (2022): 9965-9976. https://doi.org/10.1016/j.aej.2022.03.030
[10] Falodun, Bidemi O., C. Onwubuoya, and FH Awoniran Alamu. "Magnetohydrodynamics (MHD) heat and mass transfer of Casson fluid flow past a semi-infinite vertical plate with thermophoresis effect: spectral relaxation

analysis." In *Defect and Diffusion Forum*, vol. 389, pp. 18-35. Trans Tech Publications Ltd, 2018. https://doi.org/10.4028/www.scientific.net/DDF.389.18
[11] Dash, R. K., K. N. Mehta, and G. Jayaraman. "Casson fluid flow in a pipe filled with a homogeneous porous medium." *International Journal of Engineering Science* 34, no. 10 (1996): 1145-1156. https://doi.org/10.1016/0020-7225(96)00012-2
[12] Reddy, K. Veera, Kolli Vijaya, and G. Reddy. "Buongiorno model with Brownian and thermophoretic diffusion for MHD Casson nanofluid over an inclined porous surface." *Journal of Naval Architecture & Marine Engineering* 19, no. 1 (2022): 31-45. https://doi.org/10.3329/jname.v19i1.50863
[13] Kamran, A., S. Hussain, M. Sagheer, and N. Akmal. "A numerical study of magnetohydrodynamics flow in Casson nanofluid combined with Joule heating and slip boundary conditions." *Results in Physics* 7 (2017): 3037-3048. https://doi.org/10.1016/j.rinp.2017.08.004
[14] Khalid, Asma, Ilyas Khan, Arshad Khan, and Sharidan Shafie. "Unsteady MHD free convection flow of Casson fluid past over an oscillating vertical plate embedded in a porous medium." *Engineering Science and Technology, an International Journal* 18, no. 3 (2015): 309-317. https://doi.org/10.1016/j.jestch.2014.12.006
[15] Bejawada, Shankar Goud, Yanala Dharmendar Reddy, Wasim Jamshed, Kottakkaran Sooppy Nisar, Abdulaziz N. Alharbi, and Ridha Chouikh. "Radiation effect on MHD Casson fluid flow over an inclined non-linear surface with chemical reaction in a Forchheimer porous medium." *Alexandria Engineering Journal* 61, no. 10 (2022): 8207-8220. https://doi.org/10.1016/j.aej.2022.01.043
[16] Kumar, P. V., Ch Sunitha, S. M. Ibrahim, and G. Lorenzini. "Outlining the Slip Effects on MHD Casson Nanofluid Flow over a Permeable Stretching Sheet in the Existence of Variable Wall Thickness." *Journal of Engineering Thermophysics* 32, no. 1 (2023): 69-88. https://doi.org/10.1134/S1810232823010071
[17] Sekhar, P. Raja, S. Sreedhar, S. Mohammed Ibrahim, and P. Vijaya Kumar. "Radiative Heat Source Fluid Flow of MHD Casson Nanofluid over A Non-Linear Inclined Surface with Soret and Dufour Effects." *CFD Letters* 15, no. 7 (2023): 42-60. https://doi.org/10.37934/cfdl.15.7.4260
[18] Priyanka, Patil, Shaimaa AM Abdelmohsen, Jagadish V. Tawade, Abdelbacki MM Ashraf, Raman Kumar, and Mahadev M. Biradar. "Multiple slip effects of MHD boundary-layer motion of a Casson nanoliquid over a penetrable linearly stretching sheet embedded in non-Darcian porous medium." *International Journal of Modern Physics B* 37, no. 03 (2023): 2350022. https://doi.org/10.1142/S0217979223500224
[19] Crane, Lawrence J. "Flow past a stretching plate." *Zeitschrift für angewandte Mathematik und Physik ZAMP* 21 (1970): 645-647. https://doi.org/10.1007/BF01587695
[20] Ullah, Imran, Ilyas Khan, and Sharidan Shafie. "MHD natural convection flow of Casson nanofluid over nonlinearly stretching sheet through porous medium with chemical reaction and thermal radiation." *Nanoscale Research Letters* 11 (2016): 1-15. https://doi.org/10.1186/s11671-016-1745-6
[21] Narender, Ganji, Kamatam Govardhan, and Gobburu Sreedhar Sarma. "Magnetohydrodynamic stagnation point on a Casson nanofluid flow over a radially stretching sheet." *Beilstein Journal of Nanotechnology* 11, no. 1 (2020): 1303-1315. https://doi.org/10.3762/bjnano.11.114
[22] Benal, Shaila S., Jagadish V. Tawade, Mahadev M. Biradar, and Haiter Lenin Allasi. "Effects of the magnetohydrodynamic flow within the boundary layer of a Jeffery fluid in a porous medium over a shrinking/stretching sheet." *Mathematical Problems in Engineering* 2022 (2022). https://doi.org/10.1155/2022/7326504
[23] Mukhopadhyay, Swati, Prativa Ranjan De, Krishnendu Bhattacharyya, and G. C. Layek. "Casson fluid flow over an unsteady stretching surface." *Ain Shams Engineering Journal* 4, no. 4 (2013): 933-938. https://doi.org/10.1016/j.asej.2013.04.004
[24] Mukhopadhyay, Swati. "Casson fluid flow and heat transfer over a nonlinearly stretching surface." *Chinese Physics B* 22, no. 7 (2013): 074701. https://doi.org/10.1088/1674-1056/22/7/074701
[25] Das, S., Akram Ali, and R. N. Jana. "Darcy-Forchheimer flow of a magneto-radiated couple stress fluid over an inclined exponentially stretching surface with Ohmic dissipation." *World Journal of Engineering* 18, no. 2 (2021): 345-360. https://doi.org/10.1108/WJE-07-2020-0258
[26] Sarkar, S., R. N. Jana, and S. Das. "Activation energy impact on radiated magneto-Sisko nanofluid flow over a stretching and slipping cylinder: entropy analysis." *Multidiscipline Modeling in Materials and Structures* 16, no. 5 (2020): 1085-1115. https://doi.org/10.1108/MMMS-09-2019-0165
[27] Asogwa, Kanayo Kenneth, B. Shankar Goud, Nehad Ali Shah, and Se-Jin Yook. "Rheology of electromagnetohydrodynamic tangent hyperbolic nanofluid over a stretching riga surface featuring dufour effect
[28] Srinivasulu, Thadakamalla, and B. Shankar Goud. "Effect of inclined magnetic field on flow, heat and mass transfer of Williamson nanofluid over a stretching sheet." *Case Studies in Thermal Engineering* 23 (2021): 100819. https://doi.org/10.1016/j.csite.2020.100819

[29] Ibrahim, S. Mohammed, P. Vijaya Kumar, and G. Lorenzini. "Influence of Thermophoresis and Brownian Motion of Nanoparticles on Radiative Chemically-Reacting MHD Hiemenz Flow over a Nonlinear Stretching Sheet with Heat Generation." *Fluid Dynamics & Materials Processing* 19, no. 4 (2023). https://doi.org/10.32604/fdmp.2022.019796

[30] Harish, Modalavalasa, Shaik Mohammed Ibrahim, Parthi Vijaya Kumar, and Giulio Lorenzini. "A Study on Effects of Thermal Radiative Dissipative MHD Non-Newtonian Nanofluid above an Elongating Sheet in Porous Medium." *Journal of Applied and Computational Mechanics* 9, no. 4 (2023): 945-954.

[31] Sekhar, P. Raja, S. Sreedhar, S. Mohammed Ibrahim, P. Vijaya Kumar, and B. Omprakash. "Numerical investigation of heat radiation on MHD viscoelastic nanofluid flow over a stretching sheet with heat source and slip conditions." *International Journal on Interactive Design and Manufacturing (IJIDeM)* (2023): 1-10. https://doi.org/10.1007/s12008-023-01407-4

[32] Swain, Kharabela, Isaac Lare Animasaun, and S. Mohammed Ibrahim. "Influence of exponential space-based heat source and Joule heating on nanofluid flow over an elongating/shrinking sheet with an inclined magnetic field." *International Journal of Ambient Energy* 43, no. 1 (2022): 4045-4057. https://doi.org/10.1080/01430750.2021.1873854

[33] Narender, G., K. Govardhan, and G. Sreedhar Sarma. "MHD Casson nanofluid past a stretching sheet with the effects of viscous dissipation, chemical reaction and heat source/sink." *Journal of Applied and Computational Mechanics* 7, no. 4 (2021): 2040-2048.

[34] Kameswaran, P. K., M. Narayana, P. Sibanda, and P. V. S. N. Murthy. "Hydromagnetic nanofluid flow due to a stretching or shrinking sheet with viscous dissipation and chemical reaction effects." *International Journal of Heat and Mass Transfer* 55, no. 25-26 (2012): 7587-7595. https://doi.org/10.1016/j.ijheatmasstransfer.2012.07.065

[35] Hayat, T., Muhammad Bilal Ashraf, S. A. Shehzad, and Ahmed Alsaedi. "Mixed convection flow of Casson nanofluid over a stretching sheet with convectively heated chemical reaction and heat source/sink." *Journal of Applied Fluid Mechanics* 8, no. 4 (2015): 803-813. https://doi.org/10.18869/acadpub.jafm.67.223.22995

[36] Goud, B. Shankar, Y. Dharmendar Reddy, V. Srinivasa Rao, and Zafar Hayat Khan. "Thermal radiation and joule heating effects on a magnetohydrodynamic Casson nanofluid flow in the presence of chemical reaction through a non-linear inclined porous stretching sheet." *Journal of Naval Architecture & Marine Engineering* 17, no. 2 (2020). https://doi.org/10.3329/jname.v17i2.49978

[37] Parida, B. C., B. K. Swain, and N. Senapati. "Mass transfer effect on viscous dissipative MHD flow of nanofluid over a stretching sheet embedded in a porous medium." *Journal of Naval Architecture & Marine Engineering* 18, no. 1 (2021). https://doi.org/10.3329/jname.v18i1.53380

[38] Kamran, Muhammad. "Heat source/sink and Newtonian heating effects on convective micropolar fluid flow over a stretching/shrinking sheet with slip flow model." *International Journal of Heat & Technology* 36, no. 2 (2018): 473-482. https://doi.org/10.18280/ijht.360212

[39] Sharanayya, and Suresh Biradar. "Magnetized Dissipative Casson Nanofluid Flow over a Stretching Sheet with Heat Source/Sink and Soret Effect Under Porous Medium." *BioNanoScience* (2023): 1-19. https://doi.org/10.1007/s12668-023-01184-0

[40] Goud, B. Shankar, P. Pramod Kumar, and Bala Siddulu Malga. "Effect of heat source on an unsteady MHD free convection flow of Casson fluid past a vertical oscillating plate in porous medium using finite element analysis." *Partial Differential Equations in Applied Mathematics* 2 (2020): 100015. https://doi.org/10.1016/j.padiff.2020.100015

[41] Reddy, Y. Dharmendar, B. Shankar Goud, Kottakkaran Sooppy Nisar, B. Alshahrani, Mona Mahmoud, and Choonkil Park. "Heat absorption/generation effect on MHD heat transfer fluid flow along a stretching cylinder with a porous medium." *Alexandria Engineering Journal* 64 (2023): 659-666. https://doi.org/10.1016/j.aej.2022.08.049